POLITECNICO DI TORINO
Repository ISTITUZIONALE

One half of the sprinting coin: the oxygen transport cascade of a 91-yr-old female world-record sprinter

Original
One half of the sprinting coin: the oxygen transport cascade of a 91-yr-old female world-record sprinter / Colosio, M., Pilotto, A.M., Ansaldo, M., Dobrzycki, I., Pellegrino, M.A., Bottinelli, R., Re, R., Botter, A., Franchi, M.V., Sundberg, C.W., Porcelli, S.. - In: JOURNAL OF APPLIED PHYSIOLOGY. - ISSN 8750-7587. - STAMPA. - 140:6(2026), pp. 1649-1657. [10.1152/japplphysiol.00279.2026]

Availability:
This version is available at: 11583/3017240 since: 2026-10-30T16:26:42Z

Publisher:
APS

Published
DOI:10.1152/japplphysiol.00279.2026

Terms of use:

This article is made available under terms and conditions as specified in the corresponding bibliographic description in the repository

Publisher copyright

(Article begins on next page)

07 November 2026

american physiological society

JOURNAL OF APPLIED PHYSIOLOGY

J Appl Physiol 140: 1649–1657, 2026.
First published May 6, 2026; doi:10.1152/japplphysiol.00279.2026

SHORT REPORT

Experiments of Nature

One half of the sprinting coin: the oxygen transport cascade of a 91-yr-old female world-record sprinter

Marta Colosio,[1,2] Andrea M. Pilotto,[1] Massimiliano Ansaldo,[1] Isabell Dobrzycki,[2] Maria Antonietta Pellegrino,[1] Roberto Bottinelli,[1,3] Rebecca Re,[4,5] Alberto Botter,[6] Martino V. Franchi,[7] Christopher W. Sundberg,[2,8]* and Simone Porcelli[1,9]*

[1]*Department of Molecular Medicine, University of Pavia, Pavia, Italy;* [2]*Division of Geriatrics and Gerontology, Department of Medicine, School of Medicine and Public Health, University of Wisconsin – Madison, Madison, Wisconsin, United States;* [3]*IRCCS Mondino Foundation, Pavia, Italy;* [4]*Department of Physics, Politecnico di Milano, Milano, Italy;* [5]*Institute for Photonics and Nanotechnologies, National Research Council, Milano, Italy;* [6]*Laboratory for Engineering of the Neuromuscular System (LISiN), Department of Electronics and Telecommunications, Politecnico di Torino, Torino, Italy;* [7]*Department of Biomedical Sciences, University of Padova, Padova, Italy;* [8]*Department of Kinesiology, School of Education, University of Wisconsin – Madison, Madison, Wisconsin, United States; and* [9]*Fondazione IRCCS Policlinico San Matteo, Pavia, Italy*

Abstract

A 91-yr-old female set the W90^{+} world record in the 200-m sprint in 2024, surpassing her previous record by 1.13 s. This study characterized her cardiorespiratory fitness, skeletal muscle oxidative capacity, fiber-type distribution, capillarization, and satellite cells and compared these outcomes, where possible, to published reference data. Cardiorespiratory responses were assessed during a ramp cycling test to exhaustion, and muscle oxidative capacity ($m\dot{V}O_2$) was determined using near-infrared spectroscopy during repetitive arterial occlusions. Fiber-type distribution, cross-sectional area, capillarization, satellite cell content and localization, and mitochondrial respiratory capacity were analyzed in a vastus lateralis biopsy. Peak oxygen uptake ($\dot{V}O_{2peak}$) was 23 mL·kg^{-1}·min^{-1} at 98 W, with a maximal heart rate of 141 beats·min^{-1} and cardiac output of 13.6 L·min^{-1}. The $m\dot{V}O_2$ recovery rate constant (k) was 1.83 min^{-1}. Fiber composition was 57% fast MyHC II fibers (50% IIa, 5% IIa-IIx, and 2% IIx), 38% slow MyHC I fibers, and 5% hybrid I-IIa fibers. MyHC I fibers were larger, more vascularized, and had satellite cells located closer to capillaries [4,267 ± 2,181 μm^2; 1.67 individual capillary-to-fiber ratio (C/F$_i$), 5.58 capillaries × 1,000 μm^{-1} capillary-to-fiber perimeter exchange index (CFPE), 1.8-μm satellite cell-to-capillary distance] than MyHC II fibers (2,752 ± 1,608 μm^2; 1.03 C/F$_i$, 4.00 capillaries × 1,000 μm^{-1} CFPE and 10.4 μm, respectively). Mitochondrial O_2 flux was 58 and 68 pmol·(s·mg)$^{-1}$ during coupled and uncoupled respiration, respectively. The athlete's cardiorespiratory and oxidative capacity resembled those of females in their 50s or younger. Collectively, her large, well-vascularized slow fibers, high proportion of fast fibers, and preserved muscle oxidative capacity likely contributed to her world record performance, illustrating the remarkable plasticity of skeletal muscle even in very advanced age.

NEW & NOTEWORTHY We report an in vivo and ex vivo characterization of cardiorespiratory fitness and muscle oxidative capacity in a 91-yr-old female who holds the W90^{+} 200-m world record. She exhibited a high muscle oxidative capacity and a muscle fiber profile with large, well-vascularized slow fibers and a relatively high proportion of fast fibers. These findings suggest that components of the oxygen transport and utilization system can be well-preserved into very advanced age in a lifelong sprinter.

aging; human physiology; master athletes; oxygen cascade; sprint world record performance

INTRODUCTION

Human physical performance declines progressively with age, affecting both endurance- and strength-related capacities (1, 2). Although this decline is often exacerbated by disuse and sedentary behavior, the study of highly active older individuals, such as master athletes, offers a rare opportunity to distinguish the effects of aging itself from those of inactivity (3). In particular, world-class master athletes serve as exceptional models for understanding how regular training may attenuate or delay age-related physiological decline (3, 4). Previous research has shown that some individuals

*C. W. Sundberg and S. Porcelli contributed equally to this work.
Correspondence: S. Porcelli (simone.porcelli@unipv.it); C. W. Sundberg (csundberg2@medicine.wisc.edu).
Submitted 25 March 2026 / Revised 3 April 2026 / Accepted 29 April 2026

8750-7587/26 Copyright © 2026 The Authors. Licensed under Creative Commons Attribution CC-BY-NC 4.0.
Published by the American Physiological Society.

Downloaded from journals.physiology.org/journal/jappl (130.192.232.211) on November 2, 2026.

can preserve cardiorespiratory fitness and neuromuscular function well into late adulthood, maintaining performance levels that vastly exceed those of their age-matched peers (3–5). However, only a very small fraction of individuals in their 90s remain physically active, and even fewer engage in structured training or competitive sport (6). Against this backdrop, the performance of a 91-yr-old female athlete who set a new W90$^+$ world record in the outdoor 200-m sprint in June 2024 with a time of 50.33 s is particularly extraordinary.

Sprint performance is determined by two complementary physiological "halves of the coin." One-half reflects the neuromuscular determinants of sprint performance, which require repeated, rapid, high-force contractions enabled by rapid motor unit recruitment and firing rates, and skeletal muscle characteristics such as a greater proportion of fast fibers, larger fiber size, and higher force- and power-generating capacity (7–9). The other half reflects the ability of the metabolic pathways to rapidly resynthesize ATP while minimizing the disruptions in metabolic homeostasis that contribute to fatigue (7, 9). Importantly, these two halves are highly interconnected, as oxygen delivery and mitochondrial oxidative capacity influence fatigue development and the ability to maintain force and power, while muscle fiber phenotype and contractile properties shape metabolic demand, mechanical output, and oxygen utilization (10). In addition, skeletal muscle capillarization is important for oxygen diffusion and metabolite clearance, while satellite cell abundance and their proximity to capillaries may contribute to muscle remodeling and maintenance of fiber size and function across the lifespan (11, 12). Although sprinting is predominantly supported by anaerobic metabolism, completing 200 m in ∼50 s requires high ATP turnover sustained for nearly 1 min, necessitating coordinated contributions from phosphocreatine breakdown, glycolysis, and oxidative metabolism (13). Thus, the world-record performance of this 91-yr-old female athlete likely reflects preservation of both neuromuscular determinants required for rapid force production and multiple components of the oxygen transport cascade, which become increasingly more important as sprint duration increases.

Oxygen consumption ($\dot{V}O_2$) depends on the integrated function of the oxygen transport cascade, from pulmonary ventilation to oxygen delivery and extraction at the muscle level, as described by the Fick principle: $\dot{V}O_2$ = cardiac output ($\dot{Q}$) × arterial–venous O_2 difference (a-vO_2diff) (14–16). Maximal $\dot{V}O_2$ declines progressively with age (∼5–10% per decade after early adulthood), largely due to reductions in maximal cardiac output driven primarily by decreases in maximal heart rate (17–20). However, peripheral determinants of oxygen utilization also can contribute, including skeletal muscle capillarization and mitochondrial oxidative capacity, which influence oxygen diffusion and utilization at the terminal step of the cascade (14). Notably, whether skeletal muscle oxidative capacity declines intrinsically with aging remains controversial, as impairments in mitochondrial respiratory function have been variably attributed to biological aging per se versus reduced physical activity or other age-related comorbidities (21, 22). Moreover, aging is typically accompanied by the preferential atrophy of the more powerful fast myosin heavy chain (MyHC) II fibers (23), whereas the more oxidative type I fibers are relatively preserved, even in sprint-trained athletes (24). Despite this understanding, the extent to which the oxygen transport cascade can be preserved in an elite sprint athlete in the tenth decade of life, particularly in females, remains largely uncharacterized.

Therefore, the aim of this study was to comprehensively characterize the in vivo and ex vivo physiological determinants of oxygen delivery and utilization in this 91-yr-old world-record sprinter, including her cardiorespiratory fitness, muscle oxidative capacity, fiber-type distribution, fiber size, capillarization, satellite cells, and mitochondrial respiratory capacity. By comparing these outcomes to published reference data, we sought to identify physiological features that may underpin her world-record sprint performance in the tenth decade of life and provide new insight into the remarkable plasticity of human skeletal muscle with very advanced age.

METHODS

A 91-yr-old female who set the W90$^+$ world records in the 200-m outdoor, and 60-, 200-, and 400-m indoor sprints volunteered to participate in this study. Her anthropometric characteristics and world-record performances are reported in Table 1. Exercise history was obtained via interview. She began sprint training at ∼20 yr of age, had an ∼15-yr interruption in competition between ages 30 and 45, and subsequently resumed ∼45 yr of structured sprint training up to the time of assessment. The athlete trains at least three times per week, with sessions typically beginning with 2–3 min of light jogging followed by several 50–60-m accelerations at ∼50% of maximal speed. More intense sessions include repeated 50–60-m sprints at ∼80% of maximal speed with ∼3 min of recovery between bouts, and occasionally longer repetitions up to 400 m with 7–8 min of recovery. In the week preceding competition, she increases intensity, performing 200 m runs near maximal speed. Her training is not rigidly structured and is adjusted based on perceived readiness, alternating between slow runs, moderate efforts, and maximal sprints, while a training partner tracks her time.

Experimental Design

All in vivo experiments were performed 1 mo after her indoor 200-m world record and 15 days before her outdoor 200-m world record in May 2024. The athlete volunteered to participate in the "Trajectory-Age" study (25) and was informed about the aims and potential risks before providing written informed consent. The study conforms to the

Table 1. *Anthropometric characteristics and sprint records of the W90+ world record holder*

Age, yr	91
Body mass, kg	58
Height, cm	155
BMI, kg·m^{-2}	23.9
60 m indoor – March 20, 2024	13.91 s
200 m indoor – March 10, 2024	51.08 s
200 m outdoor – May 5, 2024	51.47 s
200 m outdoor – June 2, 2024	50.33 s
400 m indoor – March 19, 2024	126.04 s

Downloaded from journals.physiology.org/journal/jappl (130.192.232.211) on November 2, 2026.

principles in the Declaration of Helsinki, is registered at ClinicalTrials.gov (NCT06168591), and was approved by the AVEN Ethical Committee (Emilia Romagna region, Italy; protocol #28022; study ID 283/2022/SPER/UNIPR).

Incremental Exercise Test

Cardiorespiratory fitness was assessed using a ramp-incremental cycling test performed on an electronically braked cycle ergometer (LC-6, Monark, Sweden). Power output increased continuously at a rate of 0.2 $W \cdot s^{-1}$. The participant was instructed to maintain a constant cadence between 70 and 75 rpm, and volitional exhaustion was defined as the point at which she could no longer maintain this cadence despite strong verbal encouragement. Pulmonary ventilation ($\dot{V}_E$), O_2 uptake ($\dot{V}O_2$), and CO_2 output ($\dot{V}CO_2$) were measured breath-by-breath using a metabolic cart (Vyntus CPX, Vyaire medical GmH, Germany), which was calibrated before the test according to the manufacturer's instructions. Respiratory exchange ratio (RER) was calculated as $\dot{V}CO_2/\dot{V}O_2$. Gas exchange threshold (GET) was determined independently by two investigators using the modified "V-slope" method (26). Heart rate (HR) was recorded continuously using a 12-lead ECG (Vyntus ECG, Vyaire medical GmH, Germany). Cardiac output (CO) and stroke volume (SV) were evaluated using trans-thoracic impedance cardiography (PhysioFlow, Manatec, France). Ratings of perceived exertion (RPE) were obtained using the Borg 6–20 scale (27).

Relative concentrations of deoxygenated hemoglobin and myoglobin (HHbMb) and oxygenated hemoglobin and myoglobin ($HbMbO_2$) of the vastus lateralis were monitored using continuous wave near-infrared spectroscopy (NIRS; PortaLite, Artinis, The Netherlands), referenced to an arbitrary initial value set to zero. The probe was secured over the distal third of the vastus lateralis (~10 cm proximal to the knee joint) of the right limb, aligned parallel to the long axis of the thigh, and fixed to the skin with adhesive tape. Black elastic bandages were applied to shield the probe from ambient light. The peak change in HHbMb ($\Delta[HHbMb]_{peak}$), expressed as a percentage of the maximal deoxygenation obtained at rest during arterial occlusion (250–300 mmHg cuff inflation applied at the inguinal crease until HHbMb reached a plateau), was used as an index of fractional O_2 extraction of the muscle (28).

Data were analyzed with Excel (Office 365, Microsoft Inc., Redmond, WA) and Prism 8.0 (GraphPad, Software Inc., CA). Breath-by-breath $\dot{V}_E$, $\dot{V}O_2$, and $\dot{V}CO_2$ data were screened to exclude errant breaths (e.g., coughing, swallowing, sighing, etc.), and values exceeding 4 SD from the local mean were excluded. Peak power output (W_{peak}) was defined as the highest power output achieved before task failure. Peak cardiopulmonary variables were calculated as the highest 20 s mean obtained before exhaustion.

Muscle Oxidative Capacity by NIRS

Oxygenation changes of the right vastus lateralis were sampled at 10 Hz by a wireless, portable, and continuous wave NIRS (PortaLite, Artinis Medical Systems). While the participant was seated on the cycle ergometer, a 13 × 85-cm rapid-inflation pressure-cuff (SC12D, Hokanson) was placed distally on the thigh and attached to an electronically controlled rapid cuff-inflator (E20, Hokanson). The tissue saturation index (TSI, %) was measured using the SRS approach (29).

Baseline values were measured over 2 min of rest, and subsequently, a prolonged arterial occlusion (300 mmHg) was performed until TSI plateaued. The cuff was instantly deflated, and muscle reoxygenation was recorded until a steady state was reached (~3 min). This procedure identified the physiological normalization (PN) of TSI under resting conditions, considering the TSI plateau (TSI_{min}) as 0% and the TSI peak during reperfusion (TSI_{max}) as 100% (30). Then, the world record holder performed a moderate-intensity cycling exercise at 40 W for 5 min followed by several intermittent arterial occlusions at 300 mmHg. Duration and timing of the repeated occlusions were controlled by the investigator to maintain TSI between 50% and 60% of PN, thereby enabling assessment of muscle oxidative capacity under conditions of nonlimiting O_2 availability (31). The rate of muscle desaturation during each intermittent arterial occlusion (TSI $\%\cdot s^{-1}$) was determined using linear regression, with slopes plotted against time. Data were quality-checked before curve fitting to remove invalid values or outliers (e.g., low initial TSI values or incomplete occlusions) (32). Muscle oxidative capacity ($m\dot{V}O_2$) was estimated using exponential fitting of the recovery rate constant (k, min^{-1}), and calculated as previously described (30, 31).

Muscle Biopsy

A resting muscle biopsy was obtained from the vastus lateralis using a 130 mm Weil-Blakesley rongeur conchotome (NDB-2, Fehling Instruments, GmbH&Co, Germany) under local anesthesia (2% lidocaine) applied to the skin and muscle fascia. A 1.0–1.5-cm incision was made through the skin, subcutaneous tissue, and muscle fascia, and ~100 mg of tissue was harvested. Immediately after excision, fiber bundles were separated longitudinally under a dissecting microscope. One bundle was placed in fresh glycerol skinning solution and stored at −20°C for 3 wk to complete the single-fiber contractile experiments reported in the companion paper (33). The second bundle was placed in BIOPS buffer [2.77 mM CaK_2EGTA, 7.23 mM K_2EGTA, 5.77 mM Na_2ATP, 6.56 mM $MgCl_2$, 20 mM taurine, 50 mM MES (2-(N-morpholino) ethane sulfonic acid), 15 mM Na_2phosphocreatine, 20 mM imidazole, and 0.5 mM dithiothreitol adjusted to pH 7.1] and immediately used for high-resolution respirometry analysis. The remaining bundles were arranged longitudinally on small notecards, frozen in liquid nitrogen-cooled isopentane, and stored at −80°C for immunohistochemistry and additional molecular analyses.

High-Resolution Respirometry

For HRR analysis, muscle fibers were dissected free of connective tissue and fat and mechanically separated with fine-tipped forceps in ice-cold BIOPS buffer. The plasma membrane was permeabilized by gentle agitation for 30 min at 4°C in 2 mL of BIOPS buffer containing 20 $\mu g \cdot mL^{-1}$ saponin, followed by a 10-min wash in MiR05 medium containing 0.5 mM EGTA, 3 mM $MgCl_2$, 60 mM lactobionic acid, 20 mM taurine, 10 mM KH_2PO_4, 20 mM HEPES [4-(2-hydroxyethyl)-piperazine-1-ethanesulfonic acid], 110 mM D-sucrose, and 1

Downloaded from journals.physiology.org/journal/jappl (130.192.232.211) on November 2, 2026.

$g \cdot L^{-1}$ bovine serum albumin (BSA), essentially fatty acid-free (pH 7.1) (34). Permeabilized fibers were then weighed, and mitochondrial respiration was evaluated by measuring O_2 flux ($\dot{J}O_2$) polarographically (34). Analyses were performed in triplicate (from 3 to 6 mg wet weight of muscle fibers per analysis) in 2 mL of MiR05 at 37°C containing myosin II-ATPase inhibitor (25 µM blebbistatin dissolved in DMSO 5 mM stock) to inhibit contraction (35), using the high-resolution Oxygraph-2k (Oroboros, Austria). Oxygen concentration and flux were recorded using DatLab4 software (Oroboros Instruments, Austria). Polarographic oxygen flux ($\dot{J}O_2$) measurements were acquired at 2-s intervals with the steady-state respiration rates calculated from a minimum of 40 data points and expressed as $pmol \cdot s^{-1} \cdot mg^{-1}$ wet weight. Chamber O_2 concentration was maintained between 250 and 450 $nmol \cdot mL^{-1}$ (average O_2 partial pressure 250 mmHg) to prevent O_2 limitation (34). Standardized instrumental and chemical calibrations were performed to correct for back-diffusion of O_2 into the chamber from the various components (e.g., leak from the exterior, O_2 consumption by the chemical medium, and by the O_2 sensor) (34).

A substrate-uncoupler-inhibitor titration protocol (SUIT) was used (34). Glutamate (10 mM) and malate (4 mM) were added to assess LEAK respiration through complex I (CI_L). Submaximal titration of ADP (2.5, 5,10, 25, 50, 100, 175, 250, 500, 1,000, 2,000, 4,000, 6,000, 8,000, and 10,000 µM) was added to measure the ADP sensitivity sustained by complex I. Apparent Km ([ADP]) providing 50% of the maximum mass-specific $\dot{J}O_2$ was calculated by using a Michaelis–Menten kinetic equation (36). ADP (10 mM) was added to assess maximal oxidative phosphorylation (OXPHOS) capacity through CI (CI_P). Succinate (10 mm) was added to assess OXPHOS capacity through CI + complex II ($CI + II_P$). Cytochrome *c* (10 µM) was added to test for outer mitochondrial membrane integrity. Stepwise additions of carbonyl cyanide *p*-trifluoromethoxyphenylhydrazone (FCCP; 0.5–1.5 µM) were used to measure electron transport system (ETS) capacity through CI + II ($CI + II_E$). Inhibition of CI by rotenone (1 µM) determined electron transport system capacity through CII (CII_E), whereas addition of antimycin A (2.5 µM), inhibitor of complex III, was used to measure residual oxygen consumption, which was subtracted from all measurements.

Following each experiment, muscle samples were removed from the chamber, washed in PBS two times for 10 min in a centrifuge (13,500 rpm), and then stored at −80°C for subsequent determination of citrate synthase (CS) activity. Results were expressed relative to muscle wet weight ($pmol \cdot s^{-1} \cdot mg^{-1}$; mean of duplicate measurements) and normalized to CS activity ($pmol \cdot s^{-1} \cdot mg^{-1} \cdot CSact^{-1}$).

Citrate Synthase Activity

CS activity was determined by using the Citrate Synthase Activity Assay kit (Merck, Darmstadt, Germany). Muscle samples were homogenized in an ice-cold CS assay buffer, kept on ice for 40 min and centrifuged at 10,000 *g* for 20 min at 4°C to obtain a protein extract. Protein concentration was then determined using the RC-DC protein assay (Bio-rad Hercules, California), and 5 µg of protein lysate was used to test CS activity. After adding the appropriate Reaction Mix, the absorbance was measured at 412 nm at the initial time ($T_{initial}$) with a plate Reader (CLARIOstar Plus, BMG Labtech, Germany) and then the reaction was followed for 45 min taking an absorbance measurement (A412) every 5 min. CS enzyme activity was calculated by interpolating the reading at the final time (T_{final}) on a standard curve generated using scalar concentrations of a GSH standard solution of known concentration ($2\ nmol \cdot \mu L^{-1}$).

Immunohistochemistry

Immunohistochemical analysis was performed to determine the cross-sectional area (CSA), percentage distribution, proportional area of each fiber type, capillarization, and satellite cell content and localization. Muscle tissue was equilibrated to the cryostat (HM525NX, ThermoScientific) temperature of −21°C for ≥30 min, oriented upright and exposed in Neg-50 (Ref. 6502, Epredia), and then cross-sectioned at 7 µm with a low-profile disposable microtome blade (Ref. 3053835, Epredia) at a 10° clearance angle. Muscle sections were picked up with Superfrost Plus slides (Ref. 6776214, Epredia), air-dried at room temperature (RT) for ≥1 h, and stored at −80°C. On the day of staining for myosin heavy chain (MyHC) distribution, slides were taken from −80°C, air-dried for ≥30 min at RT, and sections circled with an ImmEdge pen (H-4000, Vector Laboratories), allowing ≥15 min to air-dry and establish a hydrophobic barrier. After rehydration in a Coplin staining jar with 3 × 5-min washes of 1X phosphate-buffered saline (PBS) at pH 7.4, muscle sections were incubated in a humidified slide stain tray (M918-2, Simport Scientific) with a primary antibody cocktail (Supplemental Table S1) and 1X PBS for 90 min at RT. Muscle sections were then washed in a Coplin staining jar 3 × 5-min each with fresh 1X PBS and subsequently incubated in a secondary antibody (Supplemental Table S1), and 1X PBS for 60 min at RT. Sections were again washed 3 × 5-min with fresh 1X PBS, mounted with 1:1 1X PBS/glycerol (5092-02, Macron Fine Chemicals), and coverslipped with a micro cover glass (48393-221, VWR). Coverslips were sealed onto the slides with clear nail polish and then stored at 4°C until imaging.

For the capillary and satellite cell staining and analysis, slides were taken from −80°C, air-dried for ≥30 min at RT, and sections circled with an ImmEdge pen (H-4000, Vector Laboratories), allowing ≥15 min to air-dry and establish a hydrophobic barrier. Tissue fixation was performed in ice-cold acetone (−20°C) for 3 min, followed by three 3-min washes in 1X PBS. Endogenous peroxidase activity was quenched by incubation with 3% hydrogen peroxide in 1X PBS for 7 min at RT. Sections were subsequently washed three times in 1X PBS and blocked for 1 h at RT in 2.5% normal horse serum (NHS; Vector Laboratories, S-2012). After blocking, sections were incubated for 90 min at RT with the following primary antibodies diluted in 2.5% NHS (Supplemental Table S1). The next day, slides were washed 4 × 5 min in 1X PBS and incubated for 90 min with biotin-SP-conjugated goat anti-Ms IgG1 (1:1,000, Jackson ImmunoResearch 115-065-205) diluted in 2.5% NHS at RT. After three additional 1X PBS washes for 3 min, sections were incubated for 1 h at RT with

Downloaded from journals.physiology.org/journal/jappl (130.192.232.211) on November 2, 2026.

the following secondary antibodies diluted in 1X PBS (Supplemental Table S1). Slides were washed three times for 5 min in 1X PBS, followed by a 20-min incubation at RT with SuperBoost Tyramide Signal Amplification Alexa Fluor 647 (1:500, ThermoFisher B40958) diluted in 1X PBS. Sections were then washed 3 × 5 min in 1X PBS and stained with DAPI (1:10,000 in 1X PBS; Thermo Fisher D1306) for 10 min at RT. After a final series of 3 × 5-min PBS washes, slides were mounted with 1:1 1X PBS/glycerol (5092-02, Macron Fine Chemicals) and coverslipped with a micro cover glass (48393-221, VWR). Coverslips were sealed onto the slides with clear nail polish and then stored at 4°C until imaging. Stained sections were visualized using fluorescence microscopy, and images were analyzed for muscle fiber typing, fiber cross-sectional area, capillarization, and satellite cell identification.

Muscle section images were acquired using a high-resolution fluorescence microscope (BZ-X810, Keyence) with a Plan Apochromat ×20 mounted objective (BZ-PA20, Keyence) and filters DAPI (49000, Chroma Technology), Cy5 (49006, Chroma Technology), FITC/Alexa Fluor 488/Fluo3/Oregon Green (49011, Chroma Technology), and CY3/TRITC (49004, Chroma Technology). Automated detection software, MyoVision (37), was used for fiber type-specific CSA and distribution analysis, with manual verification of all fibers. Capillaries and satellite cells were manually counted with ImageJ software (NIH), and all analyses were independently verified by two investigators. The proportional area of each fiber type was quantified as the fiber type-specific area (μm^2) divided by total fiber area (μm^2) multiplied by 100. Based on the methods of Hepple et al. (38), capillarization was assessed by quantifying: *i*) capillary contacts (the number of capillaries surrounding each fiber), *ii*) the capillary-to-fiber ratio on an individual fiber basis (C/F_i), and *iii*) capillary density. Capillary density was calculated using the cross-sectional area (μm^2) of each individual fiber as the reference area, and the capillary-to-fiber perimeter exchange index (CFPE) was determined as an index of capillary supply relative to a fiber's perimeter, as previously described (38). Satellite cell-to-capillary distance was measured for all satellite cells within the muscle fiber border by identifying $Pax7^+/DAPI^+$ nuclei beneath the basal lamina and determining the distance to the nearest capillary, as previously described by Nederveen et al. (12).

RESULTS

Cardiorespiratory Fitness and Muscle Oxidative Capacity

$\dot{V}O_{2peak}$ was 23 $mL \cdot kg^{-1} \cdot min^{-1}$ (1.332 $L \cdot min^{-1}$, Fig. 1*A*), achieved at a peak power output of 98 W and a RER of 1.1. At exhaustion, her heart rate reached 141 $beats \cdot min^{-1}$ [98% age-predicted, Fig. 1*B* (39)], stroke volume was 96 mL, and estimated cardiac output was 13.6 $L \cdot min^{-1}$ (Fig. 1*C*). Based on the Fick principle, the calculated arterial-venous O_2 difference was 9.7 $mL \cdot 100\ mL^{-1}$, and NIRS-derived muscle O_2 extraction from the vastus lateralis was 45%. Her end exercise ventilation ($\dot{V}E$) was 63.5 $L \cdot min^{-1}$, $\dot{V}E/\dot{V}CO_2$ was 39.6, and final RPE was 16. Her gas exchange threshold occurred at 1.092 $L \cdot min^{-1}$ (82% of $\dot{V}O_{2peak}$) at 70 W, and her respiratory compensation point occurred at 1.212 $L \cdot min^{-1}$ (91% of her $\dot{V}O_{2peak}$) at 80 W. The test was considered maximal based on the following criteria: RPE > 15, peak HR > 95% of the age-predicted maximum, and RER ≥ 1.1 (26).

During the prolonged arterial occlusion, her tissue saturation index (TSI) ranged from 45.3% (TSI_{min}) to 57.8% (TSI_{max}), yielding a total perturbation amplitude of 12.5%. The $m\dot{V}O_2$ recovery rate constant (*k*) was 1.83 min^{-1} (Fig. 2*A*).

Mitochondrial Respiration and Citrate Synthase Activity

Data from complex I- and II-coupled respiration in OXPHOS are reported in Fig. 2*B*. Citrate synthase activity was 0.30 $\mu mol \cdot mL^{-1} \cdot min^{-1}$. During CI leak respiration, O_2 flux was 1.8 $pmol \cdot s^{-1} \cdot mg^{-1}$ (7.1 $pmol \cdot s^{-1} \cdot mg^{-1} \cdot CSact^{-1}$). The CI-supported OXPHOS respiration was 27.2 $pmol \cdot s^{-1} \cdot mg^{-1}$ (99.9 $pmol \cdot s^{-1} \cdot mg^{-1} \cdot CSact^{-1}$). When CI and CII were combined during coupled OXPHOS, respiration increased to 58.9 $pmol \cdot s^{-1} \cdot mg^{-1}$ (214.6 $pmol \cdot s^{-1} \cdot mg^{-1} \cdot CSact^{-1}$). Maximal uncoupled respiration (ETS) with combined CI and CII reached 68.0 $pmol \cdot s^{-1} \cdot mg^{-1}$ (246.6 $pmol \cdot s^{-1} \cdot mg^{-1} \cdot CSact^{-1}$), while CII ETS respiration alone was 35.9 $pmol \cdot s^{-1} \cdot mg^{-1}$ (128.4 $pmol \cdot s^{-1} \cdot mg^{-1} \cdot CSact^{-1}$). Apparent Km for ADP sensitivity was 364.2 µM.

Fiber-Type CSA and Distribution

MyHC I fibers were markedly larger (4,267 ± 2,181 μm^2) than MyHC II fibers (2,752 ± 1,608 μm^2, corresponding with a type II/I ratio of 0.59 (Fig. 3, *A–D*). Despite the larger size of

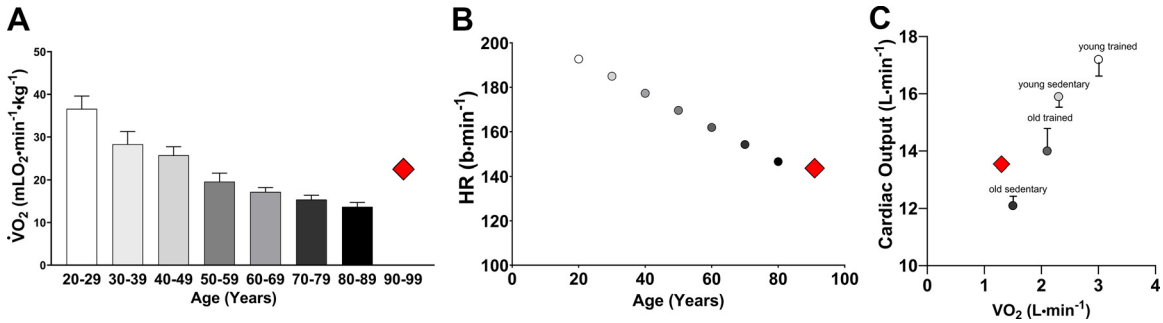


Figure 1. Cardiorespiratory fitness of the world record holder compared with reference data. All panels were adapted and modified from the original publications to improve clarity and to incorporate the data from the 91-yr-old world record holder (red diamonds). *A*: peak of oxygen consumption ($\dot{V}O_2$) compared with females performing an incremental cycling test at different ages reported by Kaminsky et al. (21). *B*: maximal heart rate (HR) compared with the linear regression between maximal HR and age in females reported by Tanaka et al. (39). *C*: maximal cardiac output at the end of the incremental cycling test compared with sedentary and trained young and older females reported by Ogawa et al. (20).

Downloaded from journals.physiology.org/journal/jappl (130.192.232.211) on November 2, 2026.

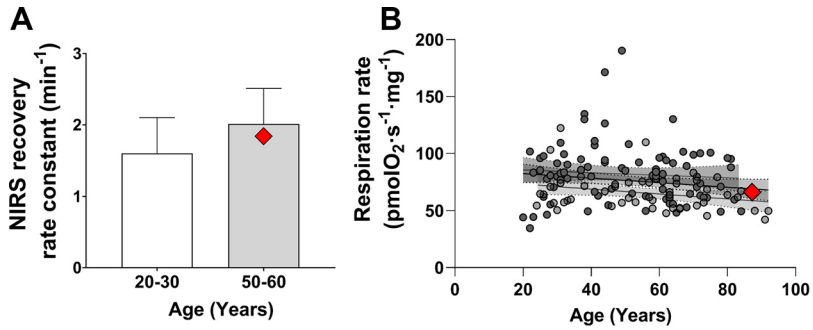


Figure 2. In vivo and ex vivo oxidative capacity of the world record holder compared with reference data. All panels were adapted and modified from the original publications to improve clarity and to incorporate the 91-yr-old world record holder (red diamonds). *A*: $m\dot{V}O_2$ recovery rate constant (*k*) by NIRS evaluated with repeated intermittent arterial occlusion compared with males and females in their 20 s and in their 50 s by Ryan et al. and Colosio et al., respectively (40, 41). *B*: mitochondrial respiration through high-resolution respirometry in complex I and II in coupled OXPHOS conditions compared with males across ages reported by Cefis et al. (42). Linear regressions represent associations between age and respiration rate for inactive and active participants separately.

MyHC I fibers, her fiber-type distribution was skewed toward a high proportion of fast fibers, with 57% fast MyHC II fibers (50% IIa, 5% IIa-IIx, and 2% IIx), 38% slow MyHC I fibers, and 5% hybrid I-IIa fibers (Fig. 3, *B–D*). As a result, the proportional fiber area was 46% MyHC II fibers (43% IIa, 2% IIa-IIx, and 1%IIx), 51% MyHC I fibers, and 3% hybrid I-IIa fibers (Fig. 3*C*).

Capillarization

MyHC I fibers were more vascularized than MyHC II fibers, as evidenced by the greater capillary contacts per fiber (4.28 vs. 2.68, respectively). The capillary-to-fiber ratio was 1.67 (C/F_i) in MyHC I fibers and 1.03 (C/F_i) in MyHC II fibers (Fig. 3, *E* and *F*). Capillary density was 300 and 283 capillaries·mm^{-2} for MyHC I and MyHC II, respectively. CFPE was 5.58 capillaries·1,000 µm^{-1} in MyHC I fibers and 4.00 capillaries·1,000 µm^{-1} in MyHC II fibers (Fig. 3, *E* and *F*).

Satellite Cells

Satellite cells were located closer to the nearest capillary in MyHC I fibers compared with MyHC II fibers (1.80 vs. 10.36 µm, respectively). Satellite cell content was also higher in MyHC I fibers, with 10.4 satellite cells per 100 fibers compared with 7.0 per 100 fibers in MyHC II fibers.

DISCUSSION

This case study represents one "half of the coin" of a broader investigation aimed at comprehensively characterizing the physiological profile of a 91-yr-old female master

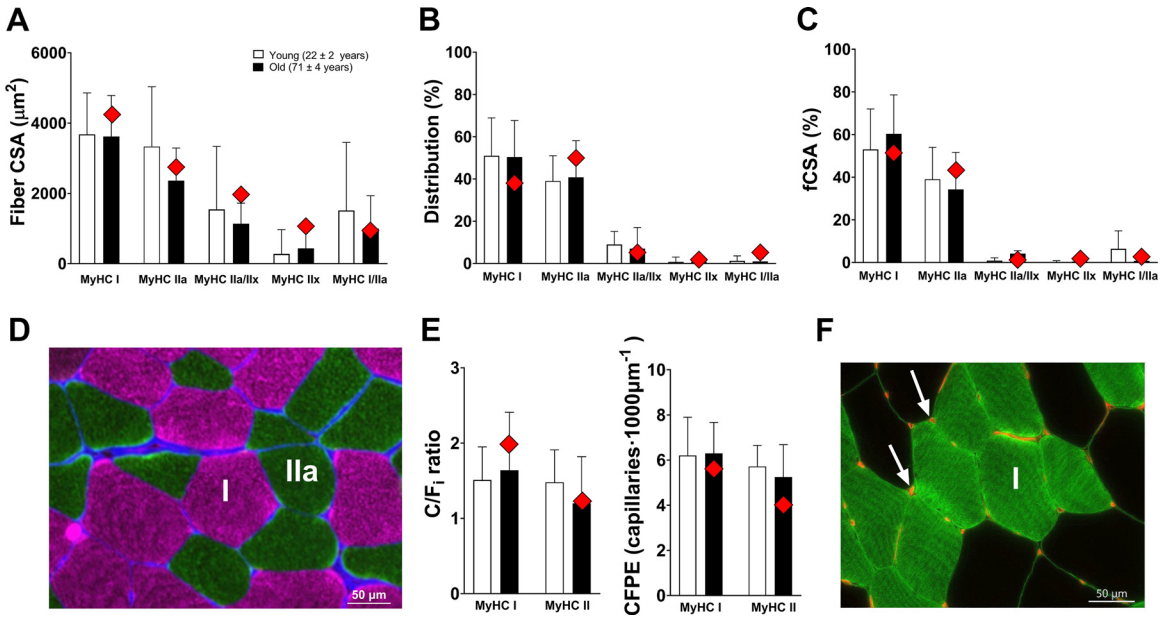


Figure 3. Fiber-type distribution and capillarization of the world record holder compared with reference data. Data from the 91-yr-old world record holder (red diamonds) are compared with young ($n = 20$; 22 ± 2 yr) and older ($n = 17$; 71 ± 4 yr) females (unpublished data from the Sundberg lab). *A*: muscle fiber cross-sectional area (CSA). *B*: fiber-type distribution (%). *C*: proportional fiber area. *D*: representative immunohistochemical image used for fiber CSA assessment in the world record holder, with MyHC I fibers stained pink and MyHC IIa fibers stained green. *E*: capillary-to-fiber ratio (C/F_i) and capillary-to-fiber perimeter exchange index (CFPE). *F*: representative image of capillary staining in the world record holder, with capillaries stained red (white arrows) and MyHC I fibers stained green.

Downloaded from journals.physiology.org/journal/jappl (130.192.232.211) on November 2, 2026.

sprinter who, in 2024, broke the world record for the 200-m sprint in the W90^{+} age category. She currently holds both the indoor (51.08 s) and outdoor (50.33 s) world records. To our knowledge, this is the first study to characterize both in vivo and ex vivo physiological characteristics of a female master sprinter of this age and performance level. The findings reveal a unique physiological profile that may contribute to her extraordinary sprint performance and provide new insight into the limits of human performance in very advanced age. Four key features emerged: *i*) cardiorespiratory fitness comparable to the 50th percentile of females in their 50s; *ii*) preserved oxidative capacity comparable to healthy females several decades younger (both in vivo and ex vivo); *iii*) exceptionally large and highly vascularized MyHC I fibers; and *iv*) a high proportion of MyHC II fibers. Collectively, this rare combination of endurance-related and power-related muscle characteristics may help explain her exceptional sprint performance in the tenth decade of life.

Oxygen Transport Cascade

Peak oxygen uptake ($\dot{V}O_{2peak}$) is a key determinant of aerobic performance and reflects the integrated functioning of the pulmonary, cardiovascular, and muscle systems to uptake, transport, and use oxygen. During the incremental cycling test (Fig. 1), the world record holder reached exhaustion near her age-predicted maximal heart rate (39), and secondary criteria (RER, HR, and RPE) supported attainment of maximal effort (26). Her $\dot{V}O_{2peak}$ was comparable to the 50th percentile of females in their 50s (21), suggesting exceptional preservation of cardiorespiratory fitness for her age, but is markedly lower than values reported in two case reports of octogenarian female endurance-trained athletes (23 mL·min^{-1}·kg^{-1} vs. 43–45 mL·min^{-1}·kg^{-1}) (43, 44). Whether this difference is driven primarily by age, training specialization (sprint vs. endurance), or methodological factors (e.g., cycle ergometry vs. treadmill testing) remains unclear. Notably, her ventilatory thresholds (both GET and RCP), expressed as a percentage of $\dot{V}O_{2peak}$, were high compared with individuals two to three decades younger (45), suggesting an ability to sustain a high fraction of her maximal aerobic capacity during prolonged high-intensity exercise.

Peak ventilation ($\dot{V}E$) appeared higher than values reported in females in their 50s and comparable to those observed in males in their 70s, while $\dot{V}E/\dot{V}CO_2$ was modestly elevated relative to both sexes in that age range (46). Together with her high gas exchange values, her estimated maximal cardiac output and stroke volume were consistent with values reported in females in their 60s (20), suggesting central circulatory function capable of supporting high metabolic demand (47). Using the Fick principle, her calculated arterial-venous O_2 difference was 9.7 mL·100 mL^{-1}, which is lower than values reported in young adults (11–14 mL·100 mL^{-1}) (48). Moreover, NIRS-derived muscle O_2 extraction during the incremental test indicated that the athlete used ~45% of her maximal O_2-carrying capacity. This value is slightly lower than that reported in females in their 30s and 50s (typically 60–100%) (40, 49), suggesting that peripheral oxygen extraction may not have been fully maximized during the test. However, given that these comparison groups were approximately half her age, the relatively modest difference indicates that peripheral oxygen extraction remained well preserved.

At the terminal step of the oxygen cascade, mitochondrial oxidative capacity determines the ability of skeletal muscle to use oxygen for ATP production. In the present study, oxidative function was assessed both in vivo using the NIRS-derived $m\dot{V}O_2$ recovery rate constant and ex vivo using high-resolution respirometry. The athlete's $m\dot{V}O_2$ recovery rate constant (Fig. 2*A*) was comparable to values reported in the vastus lateralis of healthy males and females in their 20s (41) and 50s (40) and appeared slightly higher than values reported in individuals in their late 60s (50). These observations were corroborated by high-resolution respirometry, which demonstrated preserved mitochondrial respiratory capacity (Fig. 2*B*). Her oxygen flux in the complex I + II-coupled condition was comparable to a large dataset of active young and older males (42). Similarly, her data appeared modestly lower than that of males and females in their 20s (31) but comparable to individuals in their 50s (40) and 70s (51). These findings support the growing evidence that mitochondrial capacity, while altered by inactivity, is not inevitably impaired with aging and can be well preserved with lifelong physical activity (23). Collectively, the present data demonstrate remarkable preservation across multiple components of the oxygen transport cascade in a world-record sprint athlete in her tenth decade of life, suggesting that lifelong sprint training may contribute to sustained cardiovascular health and attenuated age-related declines in oxidative capacity.

Skeletal Muscle Fiber Morphology and Microvascular Profile

The athlete's muscle fiber profile revealed a unique phenotype (Fig. 3), characterized by a relatively high proportion of MyHC II fibers exceeding what is typically observed in older females (52–54). Despite this high prevalence of MyHC II fibers, MyHC I fibers occupied the greatest proportional area due to their substantially larger size, with MyHC I fibers being ~55% larger than MyHC II fibers. This finding supports the theory that preferential type II fiber atrophy remains a prominent feature of aging (13, 55), even in elite sprint-trained master athletes (53).

One potential explanation for the preservation of large MyHC I fibers is the highly supportive microvascular and cellular environment associated with this fiber population. Capillary-to-fiber ratio and capillary-to-fiber perimeter exchange index in her MyHC I fibers were comparable to values reported in younger females in their 20s (Fig. 3, *E* and *F*) (11), and satellite cells were located markedly closer to capillaries in MyHC I fibers compared with MyHC II fibers (12). This favorable spatial organization may enhance delivery of oxygen, nutrients, and signaling factors that support fiber maintenance and remodeling, and may also improve oxygen diffusion capacity, potentially contributing to preserved oxidative function (11). In contrast, MyHC II fibers exhibited capillary-to-fiber ratio as well as capillary-to-fiber perimeter exchange index more consistent with older females in their 70s (56), and the satellite cell-capillary distance was substantially greater than in MyHC I fibers. This pattern may be particularly relevant in aging muscle, as satellite cell proximity

Downloaded from journals.physiology.org/journal/jappl (130.192.232.211) on November 2, 2026.

to capillaries has been linked to regenerative potential and muscle health (12). Collectively, the combination of large, highly vascularized MyHC I fibers alongside a high abundance of MyHC II fibers represents a rare skeletal muscle phenotype in older females that may be well suited to sustaining elite sprint performance in very advanced age.

CONCLUSION

We speculate that the athlete's extraordinary sprint performance in her tenth decade of life is attributable to a unique combination of preserved muscle oxidative capacity, high proportion of fast fibers, and exceptionally large and well-vascularized slow fibers. More broadly, this case study supports the growing evidence that physiological decline with aging is modifiable and that lifelong high-intensity exercise may promote sustained functional capacity and challenge prevailing assumptions regarding the limits of human performance in very advanced age.

DATA AVAILABILITY

Data will be made available upon reasonable request.

SUPPLEMENTAL MATERIAL

Supplemental Table S1: https://doi.org/10.6084/m9.figshare.31839442.

ACKNOWLEDGMENTS

All the authors deeply thank Emma Maria Mazzenga for precious time and effort. Moreover, we sincerely thank Prof. La Torre Antonio for fundamental help in creating this collaboration. PAX7 antibody was deposited to the DSHB by Kawakami, A. BA-D5, SC-71-s and 6H1-s antibodies were deposited to the DSHB by Schiaffino, S.

GRANTS

This study was supported by Ministero dell'Istruzione, dell'Università e della Ricerca (MIUR) Trajector-AGE (2020477RW5) and ReActiveAGE (P2022FNCPR) projects of National Interest (Italy) to M.V.F. and S.P., and a National Institutes of Health R01 grant (AG048262) to C.W.S.

DISCLOSURES

No conflicts of interest, financial or otherwise, are declared by the authors.

AUTHOR CONTRIBUTIONS

M.V.F., C.W.S., and S.P. conceived and designed research; M.C., A.M.P., M.A., I.D., M.V.F., C.W.S., and S.P. performed experiments; M.C., A.M.P., M.A., I.D., M.V.F., C.W.S., and S.P. analyzed data; M.C. and C.W.S. interpreted results of experiments; M.C. and C.W.S. prepared figures; M.C. and C.W.S. drafted manuscript; M.C., A.M.P., M.A., I.D., M.A.P., R.B., R.R., A.B., M.V.F., C.W.S., and S.P. edited and revised manuscript; M.C., A.M.P., M.A., I.D., M.A.P., R.B., R.R., A.B., M.V.F., C.W.S., and S.P. approved final version of manuscript.

REFERENCES

1. **Frontera WR**, **Hughes VA**, **Fielding RA**, **Fiatarone MA**, **Evans WJ**, **Roubenoff R.** Aging of skeletal muscle: a 12-yr longitudinal study. *J Appl Physiol (1985)* 88: 1321–1326, 2000. doi:10.1152/jappl.2000.88.4.1321.
2. **Fleg JL**, **Morrell CH**, **Bos AG**, **Brant LJ**, **Talbot LA**, **Wright JG**, **Lakatta EG.** Accelerated longitudinal decline of aerobic capacity in healthy older adults. *Circulation* 112: 674–682, 2005. doi:10.1161/CIRCULATIONAHA.105.545459.
3. **Tanaka H**, **Seals DR.** Endurance exercise performance in Masters athletes: age-associated changes and underlying physiological mechanisms. *J Physiol* 586: 55–63, 2008. doi:10.1113/jphysiol.2007.141879.
4. **Tanaka H**, **Tarumi T**, **Rittweger J.** Aging and physiological lessons from master athletes. In: *Comprehensive Physiology*. Wiley, 2019, p. 261–296.
5. **Chambers TL**, **Burnett TR**, **Raue U**, **Lee GA**, **Finch WH**, **Graham BM**, **Trappe TA**, **Trappe S.** Skeletal muscle size, function, and adiposity with lifelong aerobic exercise. *J Appl Physiol (1985)* 128: 368–378, 2020. doi:10.1152/japplphysiol.00426.2019.
6. **Kusy K**, **Zieliński J.** Aerobic capacity in speed-power athletes aged 20–90 years vs endurance runners and untrained participants. *Scand J Med Sci Sports* 24: 68–79, 2014. doi:10.1111/j.1600-0838.2012.01496.x.
7. **Bishop D**, **Girard O**, **Mendez-Villanueva A.** Repeated-sprint ability – Part II. *Sports Medicine* 41: 741–756, 2011. doi:10.2165/11590560-000000000-00000.
8. **Ross A**, **Leveritt M**, **Riek S.** Neural influences on sprint running. *Sports Medicine* 31: 409–425, 2001. doi:10.2165/00007256-200131060-00002.
9. **Bundle MW**, **Weyand PG.** Sprint exercise performance: does metabolic power matter? *Exerc Sport Sci Rev* 40: 174–182, 2012. doi:10.1097/JES.0b013e318258e1c1.
10. **Hargreaves M**, **Spriet LL.** Skeletal muscle energy metabolism during exercise. *Nat Metab* 2: 817–828, 2020 [Erratum in *Nat Metab* 2: 990, 2020]. doi:10.1038/s42255-020-0251-4.
11. **Barnouin Y**, **McPhee JS**, **Butler-Browne G**, **Bosutti A**, **De Vito G**, **Jones DA**, **Narici M**, **Behin A**, **Hogrel J**, **Degens H.** Coupling between skeletal muscle fiber size and capillarization is maintained during healthy aging. *J Cachexia Sarcopenia Muscle* 8: 647–659, 2017. doi:10.1002/jcsm.12194.
12. **Nederveen JP**, **Joanisse S**, **Snijders T**, **Ivankovic V**, **Baker SK**, **Phillips SM**, **Parise G.** Skeletal muscle satellite cells are located at a closer proximity to capillaries in healthy young compared with older men. *J Cachexia Sarcopenia Muscle* 7: 547–554, 2016. doi:10.1002/jcsm.12105.
13. **Glaister M.** Multiple Sprint Work: physiological responses, mechanisms of fatigue and the influence of aerobic fitness. *Sports Med* 35: 757–777, 2005. doi:10.2165/00007256-200535090-00003.
14. **Dominelli PB**, **Wiggins CC**, **Roy TK**, **Secomb TW**, **Curry TB**, **Joyner MJ.** The oxygen cascade during exercise in health and disease. *Mayo Clin Proc* 96: 1017–1032, 2021. doi:10.1016/j.mayocp.2020.06.063.
15. **Joyner MJ**, **Casey DP.** Regulation of increased blood flow (hyperemia) to muscles during exercise: a hierarchy of competing physiological needs. *Physiol Rev* 95: 549–601, 2015. doi:10.1152/physrev.00035.2013.
16. **Saltin B**, **Calbet JAL.** Point: In health and in a normoxic environment, $\dot{V}o_{2max}$ is limited primarily by cardiac output and locomotor muscle blood flow. *J Appl Physiol (1985)* 100: 744–745, 2006. doi:10.1152/japplphysiol.01395.2005.
17. **Robinson S.** Experimental studies of physical fitness in relation to age. *Arbeitsphysiologie* 10: 251–323, 1938. doi:10.1007/BF02011412.
18. **Higginbotham MB**, **Morris KG**, **Williams RS**, **Coleman RE**, **Cobb FR.** Physiologic basis for the age-related decline in aerobic work capacity. *Am J Cardiol* 57: 1374–1379, 1986. doi:10.1016/0002-9149(86)90221-3.
19. **Ogawa T**, **Spina RJ**, **Martin WH**, **Kohrt WM**, **Schechtman KB**, **Holloszy JO**, **Ehsani AA.** Effects of aging, sex, and physical training on cardiovascular responses to exercise. *Circulation* 86: 494–503, 1992. doi:10.1161/01.CIR.86.2.494.
20. **Kaminsky LA**, **Arena R**, **Myers J**, **Peterman JE**, **Bonikowske AR**, **Harber MP**, **Medina Inojosa JR**, **Lavie CJ**, **Squires RW.** Updated reference standards for cardiorespiratory fitness measured with cardiopulmonary exercise testing. *Mayo Clin Proc* 97: 285–293, 2022. doi:10.1016/j.mayocp.2021.08.020.
21. **Marcinek DJ**, **Ferrucci L.** Reduced oxidative capacity of skeletal muscle mitochondria IS a fundamental consequence of adult ageing. *J Physiol* 603: 17–20, 2025. doi:10.1113/JP285040.

Downloaded from journals.physiology.org/journal/jappl (130.192.232.211) on November 2, 2026.

22. **Lanza IR**, **Sundberg CW**, **Kent JA.** Reduced oxidative capacity of skeletal muscle IS NOT an inevitable consequence of adult ageing. *J Physiol* 603: 21–24, 2025. doi:10.1113/JP285042.
23. **Nilwik R**, **Snijders T**, **Leenders M**, **Groen BBL**, **van Kranenburg J**, **Verdijk LB**, **van Loon LJC.** The decline in skeletal muscle mass with aging is mainly attributed to a reduction in type II muscle fiber size. *Exp Gerontol* 48: 492–498, 2013. doi:10.1016/j.exger.2013.02.012.
24. **Korhonen MT**, **Cristea A**, **Alén M**, **Häkkinen K**, **Sipilä S**, **Mero A**, **Viitasalo JT**, **Larsson L**, **Suominen H.** Aging, muscle fiber type, and contractile function in sprint-trained athletes. *J Appl Physiol (1985)* 101: 906–917, 2006. doi:10.1152/japplphysiol.00299.2006.
25. **Lauretani F**, **Maggio M**, **Pilotto AM**, **Ansaldo M**, **Brusco CM**, **Carbonaro M**, **Amendola C**, **Nabacino M**, **Testa C**, **Ciuni A**, **Sverzellati N**, **Zucchini I**, **Salvi M**, **Mastropietro A**, **Re R**, **Botter A**, **Franchi MV**, **Porcelli S.** The trajectories of neuromuscular aging (TRAJECTOR AGE Clinical Trial): study rationale and methodological protocol. *J Am Geriatr Soc* 73: 2819–2827, 2025. doi:10.1111/jgs.70005.
26. **Beaver WL**, **Wasserman K**, **Whipp BJA**, **Whipp BJA.** A new method for detecting anaerobic threshold by gas exchange. *J Appl Physiol (1985)* 60: 2020–2027, 1986. doi:10.1152/jappl.1986.60.6.2020.
27. **Borg GAV.** Perceived exertion: a note on "history" and methods. *Med Sci Sports* 5: 90–93, 1973. doi:10.1249/00005768-197300520-00017.
28. **Grassi B**, **Pogliaghi S**, **Rampichini S**, **Quaresima V**, **Ferrari M**, **Marconi C**, **Cerretelli P.** Muscle oxygenation and pulmonary gas exchange kinetics during cycling exercise on-transitions in humans. *J Appl Physiol (1985)* 95: 149–158, 2003. doi:10.1152/japplphysiol.00695.2002.
29. **Ferrari M**, **Mottola L**, **Quaresima V.** Principles, techniques, and limitations of near infrared spectroscopy. *Can J Appl Physiol* 29: 463–487, 2004. doi:10.1139/H04-031.
30. **Adami A**, **Cao R**, **Porszasz J**, **Casaburi R**, **Rossiter HB.** Reproducibility of NIRS assessment of muscle oxidative capacity in smokers with and without COPD. *Respir Physiol Neurobiol* 235: 18–26, 2017. doi:10.1016/J.RESP.2016.09.008.
31. **Pilotto AM**, **Adami A**, **Mazzolari R**, **Brocca L**, **Crea E**, **Zuccarelli L**, **Pellegrino MA**, **Bottinelli R**, **Grassi B**, **Rossiter HB**, **Porcelli S.** Near-infrared spectroscopy estimation of combined skeletal muscle oxidative capacity and O_2 diffusion capacity in humans. *J Physiol* 600: 4153–4168, 2022. doi:10.1113/JP283267.
32. **Beever AT**, **Tripp TR**, **Zhang J**, **MacInnis MJ.** NIRS-derived skeletal muscle oxidative capacity is correlated with aerobic fitness and independent of sex. *J Appl Physiol (1985)* 129: 558–568, 2020. doi:10.1152/JAPPLPHYSIOL.00017.2020.
33. **Colosio M**, **Dobrzycki I**, **Teigen LE**, **Carbonaro M**, **Ansaldo M**, **Gatti M**, **Brusco CM**, **Canepari M**, **Bottinelli R**, **Botter A**, **Porcelli S**, **Franchi MV**, **Sundberg CW.** The other half of the sprinting coin: The neuromuscular profile of a 91-year-old female worldrecord sprinter. *J Appl Physiol (1985).* In press. doi:10.1152/japplphysiol.00280.2026.
34. **Pesta D**, **Gnaiger E.** High-resolution respirometry: OXPHOS protocols for human cells and permeabilized fibers from small biopsies of human muscle. *Methods Mol Biol* 810: 25–58, 2012. doi:10.1007/978-1-61779-382-0_3.
35. **Perry CGR**, **Kane DA**, **Lin C**, **Te Kozy R**, **Cathey BL**, **Lark DS**, **Kane CL**, **Brophy PM**, **Gavin TP**, **Anderson EJ**, **Neufer PD.** Inhibiting myosin-ATPase reveals a dynamic range of mitochondrial respiratory control in skeletal muscle. *Biochem J* 437: 215–222, 2011. doi:10.1042/BJ20110366.
36. **Zuccarelli L**, **Baldassarre G**, **Magnesa B**, **Degano C**, **Comelli M**, **Gasparini M**, **Manferdelli G**, **Marzorati M**, **Mavelli I**, **Pilotto A**, **Porcelli S**, **Rasica L**, **Šimunič B**, **Pišot R**, **Narici M**, **Grassi B.** Peripheral impairments of oxidative metabolism after a 10-day bed rest are upstream of mitochondrial respiration. *J Physiol* 599: 4813–4829, 2021. doi:10.1113/JP281800.
37. **Wen Y**, **Murach KA**, **Vechetti IJ**, **Fry CS**, **Vickery C**, **Peterson CA**, **McCarthy JJ**, **Campbell KS.** MyoVision: software for automated high-content analysis of skeletal muscle immunohistochemistry. *J Appl Physiol (1985)* 124: 40–51, 2018. doi:10.1152/japplphysiol.00762.2017.
38. **Hepple RT**, **Mackinnon SLM**, **Goodman JM**, **Thomas SG**, **Plyley MJ.** Resistance and aerobic training in older men: effects on $V_{O_2\ peak}$ and the capillary supply to skeletal muscle. *J Appl Physiol (1985)* 82: 1305–1310, 1997. doi:10.1152/jappl.1997.82.4.1305.
39. **Tanaka H**, **Monahan KD**, **Seals DR.** Age-predicted maximal heart rate revisited. *J Am Coll Cardiol* 37: 153–156, 2001. doi:10.1016/S0735-1097(00)01054-8.
40. **Colosio M**, **Brocca L**, **Gatti MF**, **Neri M**, **Crea E**, **Cadile F**, **Canepari M**, **Pellegrino MA**, **Polla B**, **Porcelli S**, **Bottinelli R.** Structural and functional impairments of skeletal muscle in patients with postacute sequelae of SARS-CoV-2 infection. *J Appl Physiol (1985)* 135: 902–917, 2023. doi:10.1152/japplphysiol.00158.2023.
41. **Ryan TE**, **Brophy P**, **Lin C**, **Hickner RC**, **Neufer PD.** Assessment of in vivo skeletal muscle mitochondrial respiratory capacity in humans by near-infrared spectroscopy: a comparison with in situ measurements. *J Physiol* 592: 3231–3241, 2014. doi:10.1113/jphysiol.2014.274456.
42. **Cefis M**, **Marcangeli V**, **Hammad R**, **Granet J**, **Leduc-Gaudet J-P**, **Gaudreau P**, **Trumpff C**, **Huang Q**, **Picard M**, **Aubertin-Leheudre M**, **Bélanger M**, **Robitaille R**, **Morais JA**, **Gouspillou G.** Impact of physical activity on physical function, mitochondrial energetics, ROS production, and Ca^{2+} handling across the adult lifespan in men. *Cell Rep Med* 6: 101968, 2025. doi:10.1016/j.xcrm.2025.101968.
43. **Cattagni T**, **Gremeaux V**, **Lepers R.** The physiological characteristics of an 83-year-old champion female master runner. *Int J Sports Physiol Perform* 15: 444–448, 2020. doi:10.1123/ijspp.2018-0879.
44. **Saillant K**, **Intzandt B**, **Bérubé B**, **Sanami S**, **Gauthier C**, **Bherer L.** Mastering the relationship between the body and the brain? The case of a female master athlete. *Exp Aging Res* 49: 372–388, 2023. doi:10.1080/0361073X.2022.2109340.
45. **Posner JD**, **Gorman KM**, **Klein HS**, **Cline CJ.** Ventilatory threshold: measurement and variation with age. *J Appl Physiol (1985)* 63: 1519–1525, 1987. doi:10.1152/jappl.1987.63.4.1519.
46. **Poulin MJ**, **Cunningham DA**, **Paterson DH**, **Rechnitzer PA**, **Ecclestone NA**, **Koval JJ.** Ventilatory response to exercise in men and women 55 to 86 years of age. *Am J Respir Crit Care Med* 149: 408–415, 1994. doi:10.1164/ajrccm.149.2.8306038.
47. **Wasserman K**, **Van Kessel AL**, **Burton GG.** Interaction of physiological mechanisms during exercise. *J Appl Physiol* 22: 71–85, 1967. doi:10.1152/jappl.1967.22.1.71.
48. **Mitchell JH**, **Sproule BJ**, **Chapman CB.** The physiological meaning of the maximal oxygen intake test. *J Clin Invest* 37: 538–547, 1958. doi:10.1172/JCI103636.
49. **Grassi B**, **Marzorati M**, **Lanfranconi F**, **Ferri A**, **Longaretti M**, **Stucchi A**, **Vago P**, **Marconi C**, **Morandi L.** Impaired oxygen extraction in metabolic myopathies: detection and quantification by near-infrared spectroscopy. *Muscle Nerve* 35: 510–520, 2007. doi:10.1002/mus.20708.
50. **Landers-Ramos RQ**, **Merriman K**, **Chartier GL**, **Parks J**, **Park H**, **Knuth ND.** Comparison of skeletal muscle oxidative function in young, middle-aged, and older males and females with similar physical activity levels. *J Appl Physiol (1985)* 136: 618–629, 2024. doi:10.1152/japplphysiol.00545.2023.
51. **Coen PM**, **Yi F**, **Lui L**, **Distefano G**, **Ramos SV**, **Goodpaster BH**, **Cawthon PM**, **Hepple RT**, **Kritchevsky SB**, **Cummings SR**, **Tranah GJ**, **Newman AB**, **DeLany JP.** Muscle mitochondrial respiration and cardiorespiratory fitness contribute to slower walking speed of older individuals who identify as black. *Aging Cell* 24: e70040, 2025. doi:10.1111/acel.70040.
52. **Teigen LE**, **Zepeda CS**, **Dobrzycki I**, **Hunter SK**, **Fitts RH**, **Sundberg CW.** Effects of acidosis and inorganic phosphate on Ca^{2+} sensitivity of young and older adult skeletal muscle fibers. *Am J Physiol Cell Physiol* 330: C224–C237, 2026. doi:10.1152/ajpcell.00445.2025.
53. **Sonjak V**, **Jacob K**, **Morais JA**, **Rivera-Zengotita M**, **Spendiff S**, **Spake C**, **Taivassalo T**, **Chevalier S**, **Hepple RT.** Fidelity of muscle fibre reinnervation modulates ageing muscle impact in elderly women. *J Physiol* 597: 5009–5023, 2019. doi:10.1113/JP278261.
54. **James JJ**, **Mellow ML**, **Bueckers EP**, **Gutsch SB**, **Wrucke DJ**, **Pearson AG**, **Smith AE**, **Hunter SK.** Sex differences in human skeletal muscle fiber types and the influence of age, physical activity, and muscle group: a systematic review and meta-analysis. *Physiol Rep* 13: e70616, 2025. doi:10.14814/phy2.70616.
55. **Grosicki GJ**, **Zepeda CS**, **Sundberg CW.** Single muscle fibre contractile function with ageing. *J Physiol* 600: 5005–5026, 2022. doi:10.1113/JP282298.
56. **Gries KJ**, **Raue U**, **Perkins RK**, **Lavin KM**, **Overstreet BS**, **D'Acquisto LJ**, **Graham B**, **Finch WH**, **Kaminsky LA**, **Trappe TA**, **Trappe S.** Cardiovascular and skeletal muscle health with lifelong exercise. *J Appl Physiol (1985)* 125: 1636–1645, 2018. doi:10.1152/japplphysiol.00174.2018.

Downloaded from journals.physiology.org/journal/jappl (130.192.232.211) on November 2, 2026.